Reviews

Investigations on Adsorption of Inorganic Ions in Aqueous Solution to Some Metal Oxides, Hydroxides and a Carbonate by the X-Ray Spectroscopic Method

Hironori OHASHI,* Kotaro YONEZU, Daisuke KAWAMOTO,* and Takushi YOKOYAMA*†**

**Department of Chemistry, Faculty of Science, Kyushu University, 744 Motooka, Nishi, Fukuoka 819-0395, Japan*

***Department of Earth Resource Engineering, Faculty of Engineering, Kyushu University, 744 Motooka, Nishi, Fukuoka 819-0395, Japan*

Why does the adsorption and concentration of inorganic chemical species proceed at aqueous–solid interfaces? In this review paper, we discuss the use of X-ray chemical state analysis to elucidate the intrinsic adsorption mechanism. Based on the chemical states of the species adsorbed to solids as determined by X-ray chemical state analysis, possible adsorption mechanisms are discussed. The driving forces of adsorption are represented by the Gibbs free energy change ($\Delta G_{chem} = \Delta G_{chem,1} + \Delta G_{chem,2}$) resulting from the formation of covalent bonds between metal ions (M) in metal oxides or hydroxides and adsorbed species (X) (M–O–X bond, $\Delta G_{chem,1}$) and the formation of new phases consisting of M and X ($\Delta G_{chem,2}$). The concept of $\Delta G_{chem,2}$ is proposed based on the experimental results from chemical state analyses. As examples, the following investigations are discussed in this review paper: the formation of mullite precursors by the adsorption of monosilicic acid to $Al(OH)_3$, the spontaneous reduction of Au(III) to Au(0) by adsorption of Au(III) to $Al(OH)_3$, MnO_2 and $Ni(OH)_2$ and the mechanism of concentration of Co^{2+}, Tl^{+}, Pb^{2+}, Pt^{2+}, Au^{+}, and Pd^{2+} in marine ferromanganese crusts.

Keywords Adsorption mechanism, adsorption driving force, solid–aqueous interface, X-ray chemical state analysis

(Received December 23, 2020; Accepted March 5, 2021; Published October 10, 2021)

† To whom correspondence should be addressed.
E-mail: yokoyamatakushi@chem.kyushu-univ.jp
Present address: Geothermal Buisiness Division, WJEC, 1-1-1, Watanabe-dori, Chuo, Fukuoka 810-0004, Japan.

H. O. present address: Faculty of Symbiotic Systems Science, Fukushima University, 1 Kanayagawa, Fukushima 960-1296, Japan.
D. K. present address: Department of Chemistry, Faculty of Science, Okayama University of Science, 1-1 Ridai-cho, Kita, Okayama 700–0000, Japan.

1 Introduction

The adsorption of chemical species to solids from aqueous solutions is an important chemical process. For example, in the geochemistry of the hydrosphere, the cycling of inorganic trace elements is controlled by adsorption at the interfaces between minerals and natural water; in environmental chemistry, undesired inorganic species are removed from water by adsorption to solid adsorbents; and, in catalytic chemistry, the catalysts such as gold or platinum clusters supported on metal oxides (called environmental catalysts) are prepared by the adsorption of metal ions on solid supports.

Until 1980, the adsorption of inorganic species had been macroscopically investigated from the viewpoint of chemical thermodynamics, and the adsorption type and adsorption capacity had mainly been examined using adsorption isotherms. In addition, the adsorption kinetics had also been investigated for the estimation of the adsorption rate and activation energy. From a practical viewpoint, these data are useful for the chemical industry.

A classic definition of adsorption is that the concentration of a chemical species on the surface of an adsorbent is higher than that in the bulk solution. However, the chemical state of the adsorbed inorganic species has scarcely been considered because of difficulty in analyzing the chemical states. Thus, in many cases, the adsorption mechanism has only been speculated. To elucidate the detailed adsorption mechanism, it is essential to investigate the chemical state of inorganic species adsorbed on solid adsorbents. Since around 1980, spectroscopic methods such as X-ray photoelectron spectroscopy (XPS), nuclear magnetic resonance (NMR), and Mössbauer spectroscopy have been applied to the microscopic investigation of adsorption, as described in this paper. In addition, synchrotron radiation facilities, such as KEK and SPring-8 in Japan, have become more easily available since the turn of the millennium, and X-ray absorption spectroscopy (XAS) has been applied actively to the chemical state analysis of inorganic species adsorbed on solid adsorbents because of its broad applicability for many elements. XAS can give information about both the valence state and local structure (average interatomic distances and coordination numbers) of target elements. In addition, it can be applied to both amorphous solids, liquid phases, and crystalline solids. However, complete information cannot always be obtained from XAS alone, and other methods are required to complement the XAS results. In this paper, the investigation of the adsorption mechanism of inorganic species on solids by a combination of XAS and other spectroscopic methods is discussed.

Although they are not described for want of space, there are other new methods to investigate adsorption of inorganic ions in aqueous solution on solid surfaces, such as atomic force microscopy in liquid, infrared spectroscopy, X-ray crystal truncation rod scattering, *etc.*[1] Using these techniques, interesting studies have been performed.[2-5]

2 Driving Force for the Adsorption Reaction

The adsorption of ions on the surface of metal oxides and hydroxides from aqueous solutions can be described thermodynamically by Eq. (1a).[6] The term $\Delta G_{chem,2}$ as proposed by the authors, is defined by Eq. (1b) and discussed later.

$$\Delta G_{ads} = \Delta G_{coul} + \Delta G_{solv} + \Delta G_{chem} \quad (1a)$$

$$\text{Where } \Delta G_{chem} = \Delta G_{chem,1} + \Delta G_{chem,2} \quad (1b)$$

Here, ΔG_{ads} is the net change in the Gibbs free energy for the adsorption of ions on the surface of metal oxides and hydroxides, ΔG_{coul} is the Gibbs free energy change caused by electrostatic effects, ΔG_{solv} is that due to dehydration effects when hydrated ions are adsorbed on the surface of metal oxides and hydroxides, and ΔG_{chem} is that due to the formation of chemical bonds between the ion and surface of metal oxides and hydroxides ($\Delta G_{chem,1}$) or by the formation of new phases consisting of adsorbed ions and metal ions in the oxides and hydroxides ($\Delta G_{chem,2}$). In this review paper, the driving force for each adsorption reaction is considered based on the changes in the chemical states of the elements in the adsorbents and adsorbed chemical species. The concept of $\Delta G_{chem,2}$ has been proposed by our research group based on several experimental facts. We deduce that, when the amount of chemical species adsorbed exceeds a critical amount, the formation of a new phase may be initiated. Thus the quantification of $\Delta G_{chem,1}$ and $\Delta G_{chem,2}$ is an important future research direction.

3 Chemical State of Al (Al K-edge XAS and ^{27}Al MAS NMR)

3·1 Adsorption of monosilicic acid to $Al(OH)_3$: Thermodynamic interpretation

The specific adsorption of anions at mineral/aqueous solution interfaces has been explained from the correlation between the pK values of the conjugate acids of the anions and the pH values at which specific adsorption shows a marked change. On the basis of this explanation, specific adsorption depends on the ease of dissociation of the conjugate acids at the mineral surface. In this model, the pH at which the adsorption of monosilicic acid to gibbsite ($Al(OH)_3$) is greatest is consistent with the theoretical pH. However, the observed amount of adsorbed monosilicic acid is greater than the theoretical amount at other pH values, as shown in Fig. 1. This discrepancy could arise because monosilicic acid is a polybasic acid (pK_1 – pK_4). This adsorption model is called the constant capacitance model.[7]

Hironori Ohashi received his Ph.D. degree in 2007 from Kyushu University. He joined the research group at Tokyo Metropolitan University (2007 – 2010), Kyushu University (2010 – 2015) and Fukushima University (2015 –). His research interests are in state analysis for supported gold-nanoparticle catalysts using Mössbauer spectroscopy and XAFS. Recently, he started a new research on material synthesis for final storage of radioactive cesium and its characterization using XRD and XAFS.

Kotaro Yonezu received his Ph.D. degree in 2009 from Kyushu University. He has worked at the Department of Earth Resources Engineering, Faculty of Engineering, Kyushu University as Assistant Professor (2010 – 2014) and Associate Professor (2014 –). His research interests are geochemistry of ore formation (Au, Cu, REE, *etc.*) and geothermal system including silica scaling based on both geo-analytical technique (ICP-MS, EPMA, XRF, XRD, XPS, XAFS, *etc.*) and field observation.

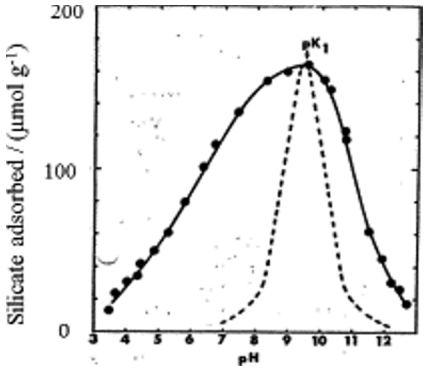

Fig. 1 Adsorption of silicate ions on gibbsite ($Al(OH)_3$) as a function of pH. Initial concentration of Si as silicate ions: 33 ppm. Amount of $Al(OH)_3$ added to 25 cm^3 of 0.1 mol dm^{-3} NaCl solution: 0.149 g. Specific surface area of $Al(OH)_3$: 58 m^2/g. ● and solid line: experimental results. Dotted line: theoretical amount of silicate ion adsorbed on $Al(OH)_3$.[7]

In this model, ΔG_{chem} is not considered.

3·2 Change in chemical state of Al during the crystallization of mullite from its precursors

Before around 2000, mullite ($3Al_2O_3{\cdot}2SiO_2$) was considered a promising high-temperature structural and electronic ceramic material. Although mullite is a natural mineral, it can be produced industrially by heating a precursor composed of Al_2O_3 and SiO_2. The mullite precursor is often prepared by the coprecipitation of monosilicic acid ($Si(OH)_4$) with aluminum hydroxide ($Al(OH)_3$).[8,9] The crystallization of mullite from mullite precursors is affected by the Si/Al atomic ratio and the degree of polymerization of the silicic acid in the precursor.[10,11] When the precursor is prepared by the coprecipitation of $Si(OH)_4$ with $Al(OH)_3$, it is often difficult to control the composition and the polymerization degree of silicic acid accurately. Compared to the coprecipitation method, the adsorption method is considered to provide more accurate control over the Si/Al ratio. Yokoyama *et al.* found that monosilicic acid adsorbs rapidly on amorphous $Al(OH)_3$ until the Si/Al molar ratio reaches 1/3, that is, the composition of mullite ($3Al_2O_3{\cdot}2SiO_2$).[12] Until an Si/Al ratio of 1/3, the adsorbed silicic acid is present as monosilicic acid. Above a molar ratio of 1/3, the adsorbed monosilicic acids polymerize to form silica. In addition, the $Al(OH)_3$ reacts with the adsorbed monosilicic acid and is almost perfectly converted to aluminosilicate (a monophasic precursor).[13,14] To produce mullite with good crystallinity at low temperatures, it is important to elucidate the relationship between the chemical properties of the mullite precursor and the crystallization of mullite.

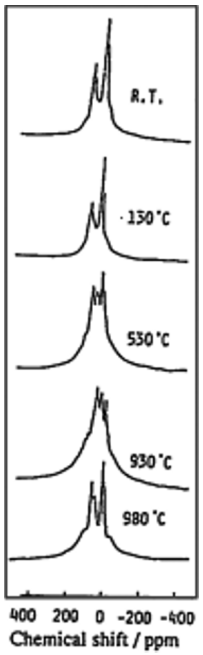

Fig. 2 ^{27}Al MAS NMR spectra for aluminum hydroxide with adsorbed silicic acid (RT: unheated) and samples heated to set temperatures. Chemical shifts relative to $[Al(H_2O)_6]^{3+}$: 0 – 30 ppm six-coordinate Al, 30 – 40 five-coordinate Al, and 40 – 80 four-coordinate Al.[16]

^{27}Al magic angle spinning (MAS) NMR spectra of samples prepared by the adsorption of $Si(OH)_4$ to $Al(OH)_3$ have been obtained. The ^{27}Al MAS NMR method can give information about the coordination number of Al, although no structural information such as the interatomic distance is included. When a sample with a Si/Al molar ratio of 1/3 is heated to 1000°C, the structure around Al changes as the temperature increases, and the crystallization of mullite occurs at approximately 980°C. To examine the changes in the structure, Al K-edge XAS data were obtained for samples heated to set temperatures (heating rate: 10°C/min) and were compared to the ^{27}Al MAS NMR spectra.[15,16] The XAS data were obtained using a laboratory X-ray absorption fine structure (XAFS) spectrometer, Technos EXAC 800. The detailed optical conditions for the measurements are shown in Table S1.

Figures 2 and 3 show the ^{27}Al MAS NMR and XAS data for gibbsite (crystalline $Al(OH)_3$, a standard six-coordinate Al species), an unheated sample, and samples heated to 130, 530, 930, and 980°C. In the Al-O system (the coordinating atoms are all oxygen), four-, five-, and six-coordinate Al can be detected

Daisuke KAWAMOTO received his Ph.D. degree in 2015 from Kyushu University. He has worked at the Department of Chemistry, Faculty of Science, Kyushu University as Research Fellow (2015 – 2017), the Department of Chemical and Biological Sciences, Faculty of Science, Japan Women's University as Assistant Professor (2017 – 2020) and the Department of Chemistry, Faculty of Science, Okayama University of Science as Lecturer (2020 –). His research interest is solid-liquid interfacial reaction between metal ions and minerals (metal oxides and carbonates).

Takushi YOKOYAMA received his Ph.D. degree in 1980 from Kyushu University. He has worked at the Department of Chemistry, Faculty of Science, Kyushu University as Assistant Professor (1980-1989), at the General Education College of Kyushu University as Associate Professor (1989 – 1994), at the Department of Chemistry, Faculty of Science, Kyushu University as Associate Professor (1995 – 2002) and as Professor (2002 – 2017). His research interest is geochemistry of silicic acid and the importance of adsorption reactions of inorganic ions in geochemistry.

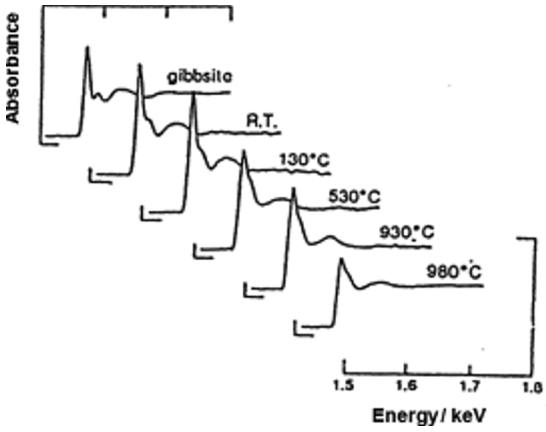

Fig. 3 Al K-edge XAS spectra for Al in aluminum hydroxide with adsorbed silicic acid (RT: unheated) and samples heated to set temperatures.[15]

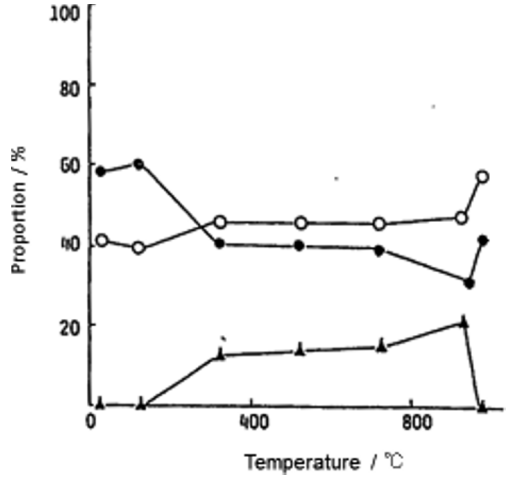

Fig. 4 Variation in the proportion for four-, five-, and six-coordinate Al in heated samples. RT: unheated, ○: four-coordinate Al, ▲: five-coordinate Al, and ●: six-coordinate Al.[16]

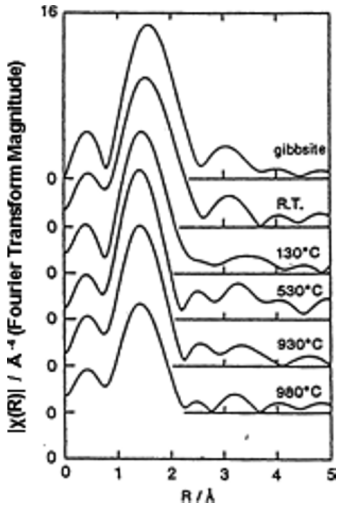

Fig. 5 Fourier transforms of EXAFS oscillations extracted from Al K-edge XAS spectra of gibbsite (standard material), an unheated sample (RT), and samples heated to set temperatures.[15]

Table 1 Al-O interatomic distance (r, Å) and coordination number (N) of aluminum in gibbsite (standard material), unheated samples, and samples heated to set temperatures[15]

Sample	r	N
Gibbsite	1.92	6[a]
RT	1.88	5.2
130°C	1.80	5.2
530°C	1.78	4.9
930°C	1.78	4.8
980°C	1.88	4.8

a. Fixed.

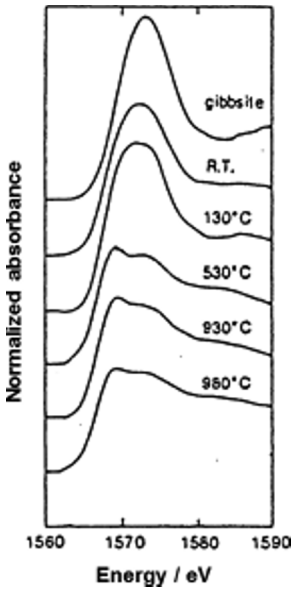

Fig. 6 Normalized Al K-edge XANES spectra for gibbsite (standard material), an unheated sample (RT), and samples heated to set temperatures.[15]

based on chemical shift relative to that of $[Al(H_2O)_6]^{3+}$. The NMR chemical shift ranges for six-, five-, and four-coordinate Al are 0 – 30, 30 – 40, and 40 – 80 ppm, respectively. Figures 4 and 5 show the changes in the proportion of four-, five-, and six-coordinate Al with temperature estimated from the NMR peak intensities and the Fourier transforms of the extended X-ray absorption fine structure (EXAFS) oscillations extracted from the Al K-edge XAS data in Fig. 3, respectively. Table 1 lists the Al-O interatomic distances (r, Å) and averaged coordination numbers (N) obtained from the EXAFS analysis. With increase in the heating temperature, both the Al-O distance and the coordination number decreased, suggesting that the proportion of six-coordinate Al decreased. In contrast, the proportion of four-coordinate Al increased, as shown in Fig. 4. The ^{27}Al MAS NMR spectra of the unheated sample and sample heated to 130°C reveal that there are two kinds of four- and six-coordinate Al species. In contrast, the samples heated to 530 and 930°C still contain five-coordinate Al, as well as four- and six-coordinate Al.[17] Figure 6 shows the X-ray absorption near edge structure (XANES) spectra of the samples. In gibbsite, all the Al ions are six-coordinate, and the peak at 1573 eV can be assigned to six-coordinate Al. The absorption edge spectra for the unheated sample and the sample heated to 130°C can be

divided into two Gaussian-shaped peaks at approximately 1570 and 1573 eV. As a result, the peak at 1570 eV can be assigned to four-coordinate Al. However, a peak corresponding to five coordinate Al was not observed in the XANES spectra. In conclusion, the changes in the Al–O distance and average coordination number with heating temperature were detected by XAS, but the appearance of five-coordinate Al was detected only by ^{27}Al MAS NMR.

Al K-edge XAS studies have been performed to examine the chemical state of Al in aluminosilicate minerals including noncrystalline mullite precursors.[18,19] Interestingly, a peak arising from five-coordinate Al was observed in the XANES spectra, and the position of the peak was located between those of four- and six-coordinate Al.[20]

In addition, XAS analysis has been applied to examine the chemical state in a natural diatoms. The results showed that the four-coordinate Al is present in the natural silica network, whereas six-coordinate Al could result from changes to the biogenic silica.[21]

3·3 What is the driving force for the adsorption of silicic acid to Al(OH)$_3$?

For the adsorption of monosilicic acid to $Al(OH)_3$, the maximum adsorption occurs at approximately pH 10. Because the isoelectric point of $Al(OH)_3$ is about pH 9, its surface charge is negative at pH 10. Consequently, neutral $Si(OH)_4$ adsorbs to the surface of $Al(OH)_3$, which is negatively charged. The electrostatic interaction between a neutral molecule and an Al–O$^-$ site may result in changes in ΔG_{coul} and ΔG_{sol}. The specific adsorption is driven by the formation of Al–O–Si bonds,[22] and the formation of the Al–O–Si bond may cause changes in ΔG_{chem}. If ΔG_{chem} is the main contribution to the formation of Al–O–Si bonds (see Eq. (1a)), the conversion of six-coordinate Al to four-coordinate Al (the formation of the mullite precursor) cannot proceed. Here, we propose that ΔG_{chem} should be divided into two factors: $\Delta G_{chem,1}$ (the formation of covalent bonds) and $\Delta G_{chem,2}$ (the formation of a new phase such as mullite precursor). A change in $\Delta G_{chem,2}$ may occur when the amount of adsorbed species (adsorption density) exceeds a critical value. In adsorption experiments of monosilicic acid to γ-Al_2O_3, ΔG_{chem} was estimated to be $-12RT$, and this corresponds to the formation of Al–O–Si bonds and the formation of aluminosilicates ($Al_2Si_{1.5}(OH)_8$ at < pH 9 and $Al_2Si_{1.5}(OH)_{7.5}O_{0.5}^{-0.5}$ at > pH 9).[23] In addition, when monosilicic acid was adsorbed to the surface of $Mg(OH)_2$, the formation of a magnesium silicate was observed.[24]

4 Chemical State of Au (Au L$_3$-edge XAS, Au 4*f* XPS and ^{197}Au Mössbauer Spectroscopy)

4·1 Importance of the adsorption of gold complex anions

Gold is generally transported in natural solutions as complexes with one or more ligands, such as Cl$^-$ and HS$^-$, depending on the environmental conditions. The adsorption of gold on mineral surfaces may be an important mechanism affecting the gold concentration in many natural solutions. Therefore, the adsorption behavior of Au(I) and Au(III) complexes on ubiquitous minerals such as iron(III) hydrous oxides, aluminum oxides and hydroxides, manganese dioxides, and silicates and carbonates has been extensively investigated.

4·2 Adsorption of Au(III) complex ions on metal oxides and hydroxides: Thermodynamic study

The gold(III) chloride ($[AuCl_4]^-$) complex is the most stable gold complex in acidic conditions (pH < 5.8) in oxidizing environments. At higher pH values, the exchange of Cl$^-$ to OH$^-$ can lead to the formation of mixed chloro-hydroxyl complexes.[25,26] Figure 7 shows a species distribution diagram of gold(III) chloride complexes in solution. However, the identities of the adsorbing species and the chemical states of the adsorbed species after adsorption are unknown. In a study of the adsorption of Au(III) complex ions on hematite (α-Fe_2O_3) by potentiometry, the adsorbed species were ≡$FeOHAuCl_3$ between pH 3 and pH 6, ≡$FeOHAuCl_2OH$ from pH 6 to pH 8, and ≡$FeOHAu(OH)_3$ above pH 8.[27] When Au(III) chloride complexes were adsorbed on goethite (FeOOH), they adsorbed specifically to the A-type hydroxyl groups on the surface of FeOOH, which act as an ideal template for bidentate coordination.[28] For the adsorption of Au(III) chloride complexes on birnessite (MnO_2), which has strong oxidation power and adsorption ability, whether and how Au(III) chloride complexes could be transformed to Au(I) complexes or Au(0) (elemental gold) is controversial.[29] Further, macroscopic modeling studies cannot verify the adsorption mode at the molecular scale, and this can only be done using appropriate molecular scale spectroscopic or scattering methods such as XAS or surface-sensitive ^{197}Au Mössbauer spectroscopy.

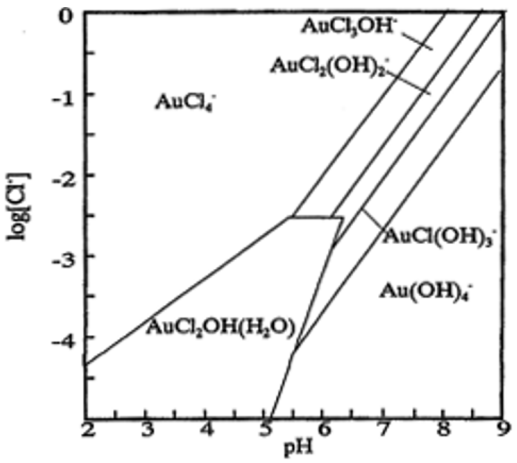

Fig. 7 Stability diagram for Au(III) species as a function of chloride concentration and pH. Total Au concentration: 1×10^{-3} mol dm^{-3}.[27]

4·3 Adsorption of Au(III) complex ions on metal oxides, hydroxides, and carbonates: Spectroscopic studies at the atomic scale

Gold coexists intimately with hydrous iron(III) and aluminum oxides that are ubiquitous in the subsurface environment. In lateritic environments, gold is often observed with goethite and bauxite. In low sulfidation gold veins, gold is often found near adularia or smectite, which might have been primarily precipitated as amorphous aluminum hydroxide, in chalcedonic or fine-grained quartz.[30] The concentration of gold complex ions to iron(III) and aluminum oxides and hydroxides from aqueous solution is considered to be a main factor affecting the formation of gold deposits. On the other hand, gold in gold ore is generally present as Au(0). How are Au(III) or Au(I) complex ions adsorbed on Fe(III) and Al oxides and hydroxides reduced? This is an interesting research theme.

In investigations into the coprecipitation of Au(III) complexes with aluminum hydroxide and iron(III) hydroxide using electron microscopy, some of the Au(III) complex ions that coprecipitated were found to have been reduced to Au(0) in the absence of a

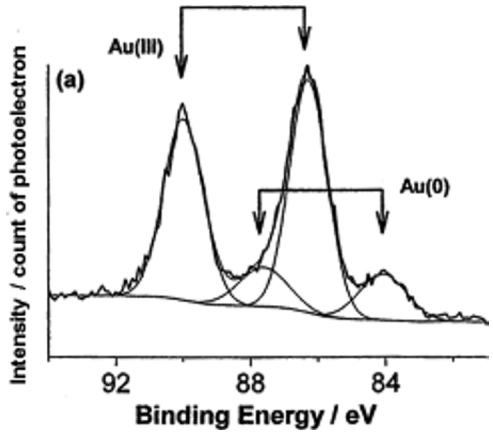

Fig. 8 Peak fitting analysis of Au XPS spectra for δ-MnO_2 after adsorption of Au(III) species. Adsorption experiment: δ-MnO_2 (250 mg) was added to Au(III) solution (500 cm^3, Au concentration: 250 ppm) with 0.12 mol dm^{-3} NaCl and adjusted to pH 6. Reaction time: 48 h. Thick line: measured spectrum. Thin line: deconvoluted spectra.[35]

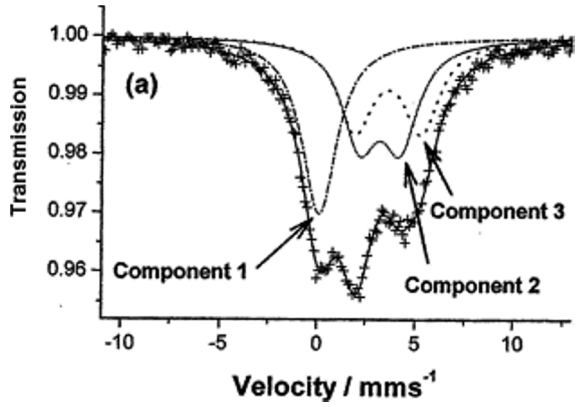

Fig. 9 Peak fitting analysis of ^{197}Au Mössbauer spectra for δ-MnO_2 after adsorption of Au(III) species. Component 1: Elemental Au (singlet). Components 2 and 3: Au(III) species, although the chemical state remains uncertain.[35]

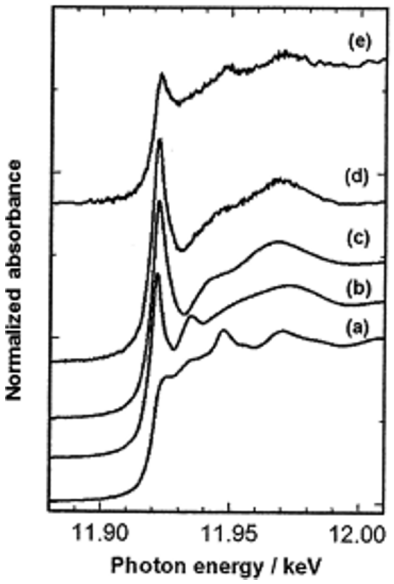

Fig. 10 Normalized Au L_3-edge XANES spectra for standard Au materials and solid samples. Standard materials: Au foil (a), $K[AuCl_4]\cdot nH_2O$ (b), and $Au(OH)_3$ (c). Samples: $NiCO_3$ and $Ni(OH)_2$ after adsorption of Au(III) species (d) and (e), respectively.[36]

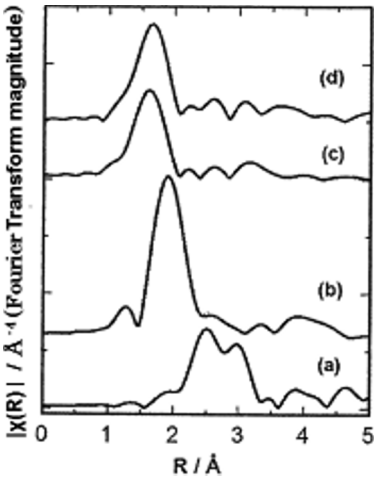

Fig. 11 Fourier transform of the EXAFS oscillations extracted from Au L_3-edge spectra. Standard materials: Au foil (a), $K[AuCl_4]\cdot nH_2O$ (b), and $Au(OH)_3$ (c). Sample: $NiCO_3$ with adsorbed Au(III) species (d).[36]

specific reducing agent.[31,32] Although Berrodier *et al.* noticed that some Au(III) complex ions had adsorbed on iron(III)- and Al-(oxy)hydroxides and been reduced to Au(0), they ignored this result and excluded the samples from their study.[33] Ohashi *et al*. were first able to determine the proportion of Au(0) formed when Au(III) complex ions are adsorbed on δ-MnO_2. Figures 8 and 9 show the 4*f* Au XPS spectra and ^{197}Au Mössbauer spectra for Au species adsorbed on δ-MnO_2. Based on the spectroscopic results, only 20% of the adsorbed Au(III) was reduced to Au(0).[34,35] Ando *et al.* studied the adsorption of Au(III) chloride complex ions on nickel hydroxide ($Ni(OH)_2$) and nickel carbonate ($NiCO_3$). Figures 10 and 11 show the Au L_3-edge XANES spectra for standard materials (a–c) and samples (d and e) and the Fourier transform of the EXAFS oscillations extracted from the Au L_3-edge spectra for standard materials (a–c) and a sample, respectively. From their results, it can be concluded that the Au(III) complex ions adsorbed on $Ni(OH)_2$ were reduced to Au(0), but the Au(III) complex ions adsorbed on $NiCO_3$ as $[Au(OH)_4]^-$ were not reduced at all.[36] In the case of the adsorption of Au(III) complex ions to $Ni(OH)_2$, a high proportion of adsorbed Au(III) complex ions was reduced to Au(0) compared to those adsorbed on $Al(OH)_3$, $Fe(OH)_3$, and MnO_2.

The subsequent reaction is proposed as Eq. (2).[37] The equilibrium constant, *K*, was estimated to be $10^{10.61}$ at 25°C. Therefore, the $AuCl_4^-$ complex ion cannot be reduced in aqueous solution.

$$Au(s) + 3H^+ + 4Cl^- + 3/4O_2(g) \rightleftharpoons [AuCl_4]^- + 2/3H_2O \quad (2)$$

With increase in pH, $AuCl_4^-$ is hydrolyzed and converted to $AuCl_{4-n}(OH)_n$, which can be adsorbed specifically on the surface of metal oxides and hydroxides (Fig. 7). In a study of the

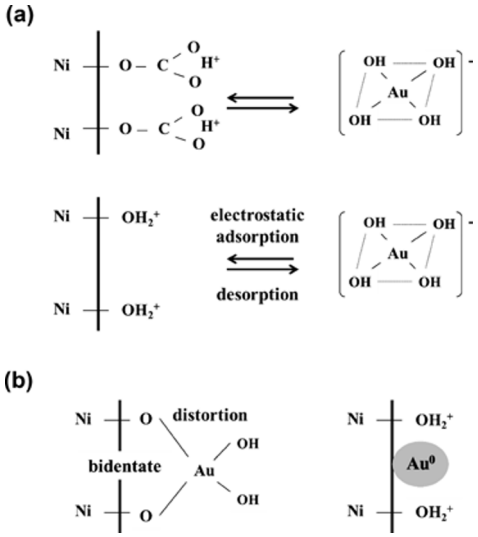

Fig. 12 Proposed models for the adsorption of Au(III) complex ions on $NiCO_3$ and $Ni(OH)_2$. First step ($NiCO_3$ and $Ni(OH)_2$) (a) and second step ($Ni(OH)_2$) (b).[36]

adsorption of Au(III) chloride complex ions on CeO_2, the Au(III) was adsorbed as mono and bidentate surface complexes, as shown below. The reduction of the Au(III) complex ions adsorbed on CeO_2 was not detected.

$$\text{Ce-OH} + \text{HOAu(OH)}_3 \longrightarrow \text{Ce-O-Au(OH)}_3 + \text{H}_2\text{O} \quad \text{(monodentate)}$$

$$\begin{array}{l} \text{Ce-OH} \\ \quad | \\ \text{O} \\ \quad | \\ \text{Ce-OH} \end{array} + (\text{HO})_2\text{Au(OH)}_2 \longrightarrow \begin{array}{l} \text{Ce-O} \\ \quad | \quad \diagdown \\ \text{O} \qquad \text{Au(OH)}_2 + 2\text{H}_2\text{O} \\ \quad | \quad \diagup \\ \text{Ce-O} \end{array} \quad \text{(bidentate)}$$

The structure of the bidentate Au(III) complex was found to be considerably distorted (unpublished data) by Au L_3 XAS (EXAFS analysis) and ^{197}Au Mössbauer spectroscopy.[38] If the $[AuCl_{4-n}(OH)_n]^-$ ion is bonded to two hydroxyl groups on the surface of metal oxide (bidentate coordination), its oxidation–reduction potential could be changed by the distortion of the coordination structure (such as the O–Au–O bond angle and Au–O bond distance). If the metal–O–Au bond is monodentate, this distortion would be very slight. As a result, the reverse reaction of Eq. (2) would occur, as shown in Eq. (3); that is, H_2O molecules would act as a reducing agent and reduce the adsorbed $AuCl_{4-n}(OH)_n$ ions to Au(0) on metal oxides and hydroxides.

$$\text{Au}^{3+}\ (\text{distorted on Ni(OH)}_2) + 3/2\text{H}_2\text{O} \longrightarrow \text{Au(0)} + 3/4\text{O}_2 + 3\text{H}^+ \quad (3)$$

As an example, a proposed model for the adsorption behavior of Au(III) complex ions on $NiCO_3$ and $Ni(OH)_2$ is shown in Fig. 12.

4·4 Standard materials for the analysis of Au(III) complexes for Au L_3-edge XAS measurements

As standard materials in the measurement of Au L_3-edge XAS data, Au foil (Au(0)), $KAu(CN)_2$ (Au(I)), and $HAuCl_4$ or $KAuCl_4{\cdot}2H_2O$ (Au(III)) are frequently used. As shown in Fig. 7, $[AuCl_4]^-$ is finally hydrolyzed to $Au(OH)_4^-$. In addition, the atoms coordinating to Au(III) complex ions adsorbed on CeO_2 are oxygen.[38] Accordingly, a Au(III) standard with oxygen atoms as the coordinating atoms is required. Thus, Kawamoto *et al.* prepared $Au(OH)_3$ and examined its chemical properties. Consequently, $Au(OH)_3$ was found to be a suitable standard material for Au(III) in the measurement of Au L_3-edge XAS data,[39] and $Au(OH)_3$ is now used as a reference standard for Au(III).[36]

4·5 What is the driving force for the adsorption of Au(III) complex ions on metal oxides and hydroxides?

The adsorption of Au(III) complex ions to $Ni(OH)_2$ and $NiCO_3$ was measured between pH 9 and 10. In this pH range, the zeta potential of $Ni(OH)_2$ and $NiCO_3$ is positive, as shown in Fig. 12, and the Au(III) complex ion is present as $Au(OH)_4^-$. The electrostatic interaction between $NiOH_3^+$ sites and $Au(OH)_4^-$ may result in the changes in ΔG_{coul} and ΔG_{sol}. After the initial electrostatic interaction, a Ni–O–Au(III) covalent bond is formed, resulting in a change in $\Delta G_{chem,1}$. Because most of the Au(III) complex ions are bidentately coordinated, they are reduced to Au(0) because of the change in $\Delta G_{chem,2}$ (reduction of Au(III) to Au(0) by H_2O). On the other hand, the Au(III) complex ion is adsorbed on the surface of $NiCO_3$ by electrostatic interactions only, which is related to ΔG_{coul}.

5 Chemical States of Some Elements in Marine Ferromanganese Deposits (XPS and XAS)

The slopes and tops of undersea mountains in the deep ocean are often covered with iron and manganese oxides, the so-called "ferromanganese crust". The marine ferromanganese crust, which is one of many types of chemical sediments in the ocean, is a sink of many elements including some rare metals. They are concentrated in the ferromanganese crust relative to seawater. The crust has been formed by the direct deposition of iron and manganese oxides from seawater. The growth rate of the crust is slow, estimated to be several millimeters every million years. Therefore, the concentration of rare metals in the deposits is considered to be caused by their adsorption on the crust from the seawater because of the long contact time.

The ferromanganese crust is regarded as a mixture of hydrous iron(III) oxides, such as goethite, and manganese dioxides, such as δ-MnO_2. Under ocean conditions, the surface charges of the iron and manganese oxides are positive and negative, respectively. The isoelectric points of iron and manganese oxides are pH 8 – 9 and pH 4, respectively. Therefore, anions can be adsorbed by the iron oxides, and cations can be adsorbed by the manganese oxides, as reported by Kochinsky and Halbach.[40] Their model was proposed based on the results of the sequential leaching of marine ferromanganese precipitates. However, the sequential leaching method often yields doubtful results because of the differences in dissolution rates of the various (Mn and Fe) crystal phases, as well as the various bonding modes of the target elements.[41] For example, which is the preferred phase for each element? This is an important problem in geochemistry. We introduce here adsorption experiments of some important rare metals concentrated in marine ferromanganese crusts and discuss the driving forces for the adsorption and concentration reactions based chemical state analysis. The order of concentrations of rare metals in marine ferromanganese crusts with respect to their concentrations in seawater is as follows: Pb >Co > Mn > Ce > Te > Y > Fe > other rare earth elements.[42]

5·1 Chemical states of cations

In 2015, a textbook about the earth science of marine

ferromanganese deposits was published. In this book, Takahashi describes in detail the application of XAS to characterize trace elements, including rare metals, in marine ferromanganese deposits.[43] Here, the chemical states of Co, Tl, Ce, and Pb in marine ferromanganese crust are discussed because of the geochemical interest in these species. The adsorption behavior of Co, Ce, Tl and Pb are described in Supporting Information 5.1 in detail.[44-55]

5·2 Chemical states of anions

As discussed above, according to the model of Kochinsky and Halbach,[40] cations are adsorbed by manganese dioxide in marine ferromanganese crust. On the other hand, Pt, Au, and Pd, which are present as anions in seawater, as discussed later, are also enriched in the ferromanganese crust.[56]

5·2·1 Platinum (Pt 4*f* XPS, Pt L_3-edge XAS)

The marine ferromanganese crust is a potential Pt resource. According to a recent study, the Pt content in marine ferromanganese crusts ranges from 44 to 3207 ppb and the averaged value is 314 ppb ($N = 182$).[57] The dissolved Pt concentration in the Pacific Ocean shows a nutrient-type profile, and the Pt concentration increases with depth, from 100 pg/L in shallow waters to approximately 300 pg/L in deeper water. Pt in seawater exists as negatively-charged complexes with OH^- and Cl^- as the dominant ligands: $[Pt(OH)_nCl_{4-n}]^{2-}$.[45]

As shown by the comparison of the Pt concentration in seawater and Pt content in the marine ferromanganese crust, Pt is extremely concentrated in the ferromanganese crust. Different mechanisms have been proposed to explain this strong enrichment, including the reduction of Pt(II) to Pt(0) or oxidation to Pt(IV) and adsorption on iron oxyhydroxide or manganese oxide phases. Until 2019, no chemical state analysis for Pt in marine ferromanganese crusts had been performed because of the low content of Pt.

In 2016, Maeno *et al.* carried out adsorption experiments of Pt(II) complex ions on δ-MnO_2 and determined the chemical state of the adsorbed Pt by Pt 4*f* XPS and XAS (Pt L_3-edge XANES and EXAFS). The results indicated that the adsorbed Pt(II) was oxidized to Pt(IV), and $[Pt(OH)_nCl_{4-n}]^{2-}$ complex ions were specifically adsorbed above pH 6 by the formation of Mn–O–Pt bonds through the condensation of Mn–OH groups in δ-MnO_2 and Pt–OH groups in the $[Pt(OH)_nCl_{4-n}]^{2-}$ complex ion. EXAFS analysis showed that the coordination structure of Pt adsorbed on δ-MnO_2 is almost the same as that of the $[Pt(OH)_6]^{2-}$ complex ion that is used as a standard. During adsorption, the release of Mn^{2+} from the δ-MnO_2 was observed. The amount of the released Mn^{2+} was similar to the amount of Pt adsorbed. Thus, the oxidative adsorption mechanism of $[Pt(OH)_nCl_{4-n}]^{2-}$ can be represented by Eq. (4).

$$MnO_2(s) + [Pt(OH)_nCl_{4-n}]^{2-} + (4 + n)H^+ \longrightarrow Mn^{2+} + Pt^{4+}(s) + (4 - n)Cl^- + (2 + n)H_2O \quad (4)$$

Here, $Pt^{4+}(s)$ means the Pt^{4+} incorporated in MnO_2 structure. The dissolved Pt^{2+} in seawater has a four-coordinate square planar structure, but Pt^{4+} has a six-coordinate octahedral structure. Through the transformation of the coordination structure of Pt(II), Pt^{4+} may substitute Mn^{4+} in $MnO_2(s)$, as shown in Fig. 13.[58]

In 2020, Koschinsky *et al.* reported the Pt L_2 and L_3-edge XANES spectra for Pt adsorbed on FeOOH and δ-MnO_2 and Pt in a natural marine ferromanganese crust. The results showed that Pt(II) adsorbed on FeOOH was not oxidized but was oxidized to Pt(IV) on δ-MnO_2. Importantly, most of Pt in the ferromanganese crust was determined to be Pt(IV).[57]

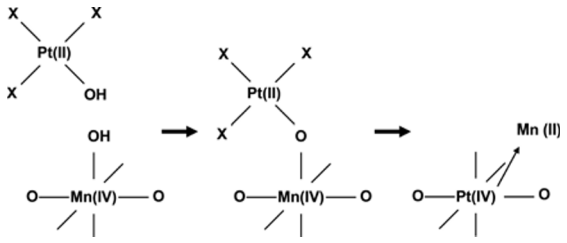

Fig. 13 Proposed mechanism for the enrichment of Pt in δ-MnO_2 through the isomorphous substitution of Pt(IV) and Mn(IV) ions. X = Cl^- and OH^-.[58]

5·2·2 Gold (Au L_3-edge XAS)

The Au content in marine ferromanganese crusts ranges from 2.5 to 397 ppb, and Au is enriched in the marine ferromanganese crust by a factor of 10^5 to 10^7 compared to its average concentration in seawater,[56] which is 29 ± 9 pg/L.[59] Au may be present as Au(I) complex ions such as $[AuCl_2]^-$ or $AuOH(H_2O)$ in seawater.[59,60] However, no chemical state analysis of Au in natural marine ferromanganese crusts has been reported to date. Yonezu *et al.* studied the adsorption behavior of $[Au(S_2O_3)_2]^{3-}$ complex ions, which are stable as Au(I) complex under oxic condition, on alumina using Au L_3-edge XANES measurements and found that the adsorbed Au(I) complexes were converted to Au(0).[61] The results suggest that the adsorbed Au(I) complex ions disproportionate to Au(0) and Au(III), as shown in Eq. (5), and the Au(III) may be reduced spontaneously to Au(0), as discussed above.

$$3[Au(S_2O_3)_2]^{3-} + (4 - n)Cl^- + nOH^- \longrightarrow 2Au(0) + [AuCl_{4-n}(OH)_n]^- + 6S_2O_3^{2-} \quad (5)$$

Au(I) complex ions are strongly adsorbed to oxides of Fe(III) and Mn(IV).[34] The adsorbed Au(I) complex ions probably disproportionate to Au(0) and Au(III) and, finally, the Au(III) complex ions are reduced to Au(0), as described above.

There is another reduction mechanism for the $[AuCl_{4-n}(OH)_n]^-$ ion in Eq. (5) in addition to spontaneous reduction. The Au(III) complexes can be coprecipitated with manganese hydroxide ($Mn(OH)_2$), followed by their stoichiometric reduction to Au(0).[62] As described above, when Co^{2+} and Tl^+ are adsorbed on δ-MnO_2, their oxidation occurs to release Mn^{2+}, which is hydrolyzed to form $Mn(OH)_2$. Then, Mn^{2+} in $Mn(OH)_2$ is oxidized to Mn^{4+}, which forms a new layer of MnO_2, and this occurs in parallel with the reduction of the Au(III) complex ions.

Pt and Au exist in seawater as complex ions of Pt(II) having a square planar structure and Au(I) having a linear structure; however, the Pt(II) complex ion is oxidized to Pt(IV) after adsorption on δ-MnO_2, whereas the Au(I) complex ion is spontaneously reduced to Au(0), as described above. Thus, it could be speculated that if the host mineral of Au is manganese oxide in marine ferromanganese crust, Au may be present as Au(0).

5·2·3 Palladium (Pd K-edge XAS)

Pd is a platinum group element. The Pd concentration in seawater ranges from 20 to 60 pg/L, and the Pt/Pd atomic ratio is about 4.5. The Pd concentration in marine ferromanganese crusts ranges from 1 to 37 ppb, and the average value is 7.3 ppb ($N = 124$), which is lower than that of Pt.[52] In contrast to that in seawater, the Pt/Pd atomic ratio of ferromanganese crust is about 87.[52] The difference in the Pt/Pd ratios between seawater

and marine ferromanganese crust is called the "Pt-Pd anomaly". Tanaka *et al.* examined the adsorption behavior of Pd complex ions on δ-MnO_2 and the chemical state of the adsorbed Pd using Pd K-edge XAS measurements. Pd was found to be present as $[PdCl_3OH]^{2-}$ complex ions in seawater,[63] and $[PCl_3OH]^{2-}$ complex ions were specifically adsorbed at pH values above 5 by the formation of a Mn–O–Pd bond through condensation between Mn–OH group on δ-MnO_2 and Pd–OH group in the $[PdCl_3OH]^{2-}$ complex ion. Through the adsorption reaction, a Cl ligand was exchanged with an O ligand (OH group). The curve fitting of the EXAFS spectra revealed the formation of two different inner-sphere complexes: bidentate-mononuclear and bidentate-binuclear complexes. However, the valence state of Pd(II) was not changed.[64]

5·3 What is the driving force for the enrichment of cations and anions in marine ferromanganese crusts?

Cations are first adsorbed on manganese dioxides by electrostatic interactions because of the negative surface charge on δ-MnO_2 under ocean condition, and this affects ΔG_{coul} and ΔG_{solv}. Secondly, inner-sphere complexes are formed through the formation of Mn–O–cation bonds causing changes in $\Delta G_{chem,1}$. In the cases of Co^{2+} and Tl^{+}, oxidation occurs from Co^{2+} to Co^{3+} and from Tl^{+} to Tl^{3+} through the Mn–O–Co^{2+} and Mn–O–Tl^{+} bonds by coupling to the reduction of Mn^{4+} to Mn^{2+}. After these redox reactions, Co^{3+} and Tl^{3+} may be incorporated in the manganese oxide structure. These redox reactions and incorporation are considered to correspond to changes in $\Delta G_{chem,2}$. In the case of Pb, although redox reactions do not occur, the formation of DES and TCS may correspond to changes in $\Delta G_{chem,2}$ as shown in Fig. S1.

In contrast to cations, anions may adsorb on δ-MnO_2 by overcoming the electrostatic repulsion between the negative charge of the anion and negative surface charge on δ-MnO_2. In this system, ΔG_{coul} may be positive and $\Delta G_{chem,1}$ and $\Delta G_{chem,2}$ may be large and negative. In the case of Pt, the oxidation of Pt^{2+} to Pt^{4+} and the substitution of Mn^{4+} by Pt^{4+} in manganese oxide occur. In the case of Au, Au^{+} disproportionates to Au^{3+} and Au(0), and the Au^{3+} is reduced spontaneously to Au(0). For Pd, ligand exchange from Cl to OH occurs. These reactions correspond to changes in $\Delta G_{chem,2}$.

6 Conclusions

The adsorption of ions from aqueous solution involves specific chemical reactions at the interface of the solid and solution and is an interesting chemical phenomenon. One of our research aims is to elucidate these adsorption mechanisms and the corresponding driving forces. To achieve this, it is essential to determine the chemical states of the adsorbed species. XAS is one of the most useful methods for chemical speciation. By determining the chemical states and structures, both the adsorption mechanism and driving forces of the adsorption reaction can be resolved.

7 Acknowledgements

The authors would like to thank Dr. Yasuhiro Kobayashi for help with the measurements of the Mössbauer spectra at the Institute for Integrated Radiation and Nuclear Science, Kyoto University. We also thank Dr. Tetsuo Honma and Dr. Takeharu Sugiyama for help in the measurement of XAS data at SPring-8 and SAGA-LS.

8 Supporting Information

XAS measurement condition (Table S1) and chemical state analysis for cations in marine manganese crust in 5.1. This material is available free of charge on the Web at http://www.jsac.or.jp/analsci/.

9 References

1. H. Sakuma and J. Kawano, *Chikyukagaku (Geochemistry)*, **2014**, *48*, 31.
2. F. Jia, X. Xhang, and S. Song, *Phys. Chem. Chem. Phys.*, **2017**, *19*, 3837.
3. K. Miyata, J. Tracy, K. Miyazawa, V. Haapasilta, P. Spijker, Y. Kawagoe, A. S. Foster, K. Tsukamoto, and T. Fukuma, *Nano Lett.*, **2017**, *17*, 4083.
4. J. Han and H. M. Ro, *Sci. Rep.*, **2019**, *9*, 6130.
5. H. Sakuma, *J. Geophys. Res. Solid Earth*, **2013**, *118*, 6066.
6. R. O. James and T. W. Healy, *J. Colloid Interface Sci.*, **1972**, *40*, 65.
7. F. J. Hingston, A. M. Posner, and J. P. Quirk, *Search*, **1970**, *1*, 324.
8. M. Inoue, H. Kominami, and T. Inui, *J. Am. Ceram. Soc.*, **1996**, *79*, 793.
9. Y. X. Huang, A. M. R. Senos, J. Rocha, and J. L. Baptista, *J. Mater. Sci.*, **1997**, *32*, 105.
10. K. Okada and N. Otsuka, *J. Am. Ceram. Soc.*, **1986**, *69*, 652.
11. W. C. Wei and J. W. Halloran, *J. Am. Ceram. Soc.*, **1988**, *71*, 166.
12. T. Yokoyama, O. Nakamura, and T. Tarutani, *Bull. Chem. Soc. Jpn.*, **1982**, *55*, 975.
13. T. Yokoyama, O. Nakamura, and T. Tarutani, *Bull. Chem. Soc. Jpn.*, **1984**, *57*, 2989.
14. T. Yokoyama, K. Nishu, S. Torii, Y. Ikeda, and T. Watanabe, *J. Mater. Sci.*, **1997**, *12*, 2111.
15. Y. Ikeda, T. Yokoyama, S. Yamashita, and H. Wakita, *Jpn. J. Appl. Phys.*, **1992**, *32*, 670.
16. Y. Ikeda, T. Yokoyama, S. Yamashita, T. Watanabe, and H. Wakita, *Adv. X-Ray Chem. Anal., Jpn*, **1996**, *27*, 211.
17. R. J. Bushby and M. P. Tytko, *J. Chem. Soc. Commun.*, **1986**, 23.
18. G. Küper, H. Peitz, I. Winter, J. Homes, H. Schneider, M. Schmücker, and D. Voll, *J. Am. Ceram. Soc.*, **1996**, *79*, 813.
19. H. Ichihashi, T. Kurisaki, T. Yamaguchi, T. Yokoyama, and H. Wakita, *Jpn. J. Appl. Phys.*, **1999**, *38*, 101.
20. D. Li, G. M. Bancroft, M. E. Eleet, X. H. Feng, and Y. Pan, *Am. Mineral.*, **1993**, *80*, 432.
21. L. Beck, M. Gehlen, A. M. Flank, A. J. Van Bennekom, and J. E. E. Van Beusekom, *Phys. Res. B*, **2002**, *189*, 180.
22. S. Goldberg, *Soil Sci. Soc. Am. J.*, **1985**, *49*, 851.
23. C. P. Huang, *Earth Planet. Sci. Lett.*, **1975**, *27*, 265.
24. H. Muraishi and S. Kitahara, *Nippon Kagaku Kaishi*, **1978**, 1457.
25. P. J. Murphy and M. S. LaGrange, *Geochim. Cosmochim. Acta*, **1998**, *62*, 3515.
26. X. Chen, W. Chu, D. Chen, Z. Wu, A. Marcelli, and Z. Wu, *Chem. Geol.*, **2009**, *268*, 74.
27. O. N. Karasyova, L. I. Ivanova, L. Z. Lakshtanov, L. Lövgren, and S. Sjöberg, *Aquat. Geochem.*, **1998**, *4*, 215.
28. M. L. Machesky, W. O. Andrade, and A. W. Rose, *Geochim. Cosmochim. Acta*, **1991**, *55*, 769.
29. Y. Ran, J. Fu, A. W. Rate, and R. J. Gilkes, *Chem. Geol.*,

2002, *185*, 33.
30. E. Izawa, Y. Urashima, K. Ibaraki, R. Suzuki, T. Yokoyama, K. Kawasaki, A. Koga, and S. Taguchi, *J. Geochem. Explor.*, **1990**, *36*, 1.
31. T. Yokoyama, Y. Matsukado, A. Uchida, Y. Motomura, K. Watanabe, and E. Izawa, *J. Colloid Interface Sci.*, **2001**, *233*, 112.
32. A. Uchida, T. Yokoyama, Y. Motomura, A. Miyazaki, Y. Okaue, K. Watanabe, and E. Izawa, *Resour. Geol.*, **2002**, *52*, 223.
33. I. Berrodier, F. Farges, M. Benedetti, M. Winterer, G. E. Brown, and M. Deveughèle, *Geochim. Cosmochim. Acta*, **2004**, *68*, 3019.
34. H. Ohashi, H. Ezoe, H. Yamashige, Y. Okaue, S. Matsuo, T. Kurisaki, H. Wakita, and T. Yokoyama*, Adv. X-Ray Chem. Anal. Jpn.*, **2005**, *36*, 339.
35. H. Ohashi, H. Ezoe, Y. Okaue, Y. Kobayashi, S. Matsuo, T. Kurisaki, A. Miyazaki, H. Wakita, and T. Yokoyama, *Anal. Sci.*, **2005**, *21*, 789.
36. H. Ando, D. Kawamoto, H. Ohashi, T. Honma, T. Ishida, Y. Okaue, M. Tokunaga, and T. Yokoyama, *Colloids Surf., A*, **2018**, *537*, 383.
37. C. H. Gammons, Y. Yu, and A. E. Williams-Janes, *Geochim. Cosmochim. Acta*, **1997**, *61*, 1971.
38. T. Yokoyama, Abstract of an annual meeting of EXAFS (Fukuoka), **2006**.
39. D. Kawamoto, H. Ando, H. Ohashi, Y. Kobayashi, T. Honma, T. Ishida, M. Tokunaga, Y. Okaue, S. Utsunomiya, and T. Yokoyama, *Bull. Chem. Soc. Jpn.*, **2016**, *11*, 1385.
40. A. Koschinsky and P. Halbach, *Geochim. Cosmochim. Acta*, **1995**, *59*, 5113.
41. S. A. Moorby and D. S. Cronan, *Geochim. Cosmochim. Acta*, **1981**, *45*, 1855.
42. J. R. Hein, A. Koschinsky, and A. N. Halliday, *Geochim. Cosmochim. Acta*, **2003**, *67*, 1117.
43. A. Usui, Y. Takahashi, T. Itou, A. Maruyama, and K. Suzuki, "*Geoscience of Marine Manganese Deposits*", **2015**, Tokyo Daigaku Jpn. (ISBN: 978-4-13-062722-1).
44. J. W. Murray, *Geochim. Cosmochim. Acta*, **1975**, *39*, 635.
45. R. H. Byrne, L. R. Kump, and K. J. Cantrell, *Mar. Chem.*, **1988**, *25*, 163.
46. R. G. Burns, *Geochim. Cosmochim. Acta*, **1976**, *40*, 95.
47. J. W. Murray and J. G. Dillard, *Geochim. Cosmochim. Acta*, **1979**, *43*, 781.
48. J. G. Dillard, D. L. Crowther and J. W. Murray, *Geochim. Cosmochim. Acta*, **1982**, *46*, 755.
49. Y. Takahashi, A. A. Manceau, N. Geoffroy, M. A. Marcus, and A. Usui, *Geochim. Cosmochim. Acta*, **2007**, *71*, 984.
50. A. Manceau, A. I. Gorshkov, and V. A. Drits, *Am. Mineral.*, **1992**, *77*, 1133.
51. A. Ohta and I. Kawabe, *Geochim. Cosmochim. Acta*, **2000**, *65*, 695.
52. Y. Takahashi, H. Shimizu, A. Usui, H. Kagi, and M. Nomura, *Geochim. Cosmochim. Acta*, **2000**, *64*, 2929.
53. J. Bebie, T. M. Seward, and J. K. Hovey, *Geochim. Cosmochim. Acta*, **1998**, *62*, 1643.
54. C. L. Peacock and E. M. Moon, *Geochim. Cosmochim. Acta*, **2012**, *84*, 297.
55. J. R. Bargar, G. E. Brown, and G. A. Parks, *Geochim. Cosmochim. Acta*, **1998**, *62*, 193.
56. V. K. Banakar, J. R. Hein, R. P. Rajani, and A. R. Chodankar, *J. Earth Syst. Sci.*, **2007**, *116*, 3.
57. A. Koschinsky, J. R. Hein, D. Kraemer, A. L. Foster, T. Kuhn, and P. Halbach, *Chem. Geol.*, **2020**, *539*, 119426.
58. M. Y. Maeno, H. Ohashi, K. Yonezu, A. Miyazaki, Y. Okaue, K. Watanabe, T. Ishida, M. Tokunaga, and T. Yokoyama, *Miner. Deposita*, **2016**, *51*, 211.
59. M. Koide, V. Hodge, E. D. Goldberg, and K. Bertine, *Appl. Geochem.*, **1988**, *3*, 237.
60. K. K. Kenison Falkner, and J. M. Edmond, *Earth Planet. Sci. Lett.*, **1990**, *98*, 208.
61. K. Yonezu, T. Yokoyama, Y. Okaue, A. Imai, and K. Watanabe, *Resour. Geol.*, **2007**, *57*, 400.
62. M. Yamashita, H. Ohashi, Y. Kobayashi, Y. Okaue, T. Kurisaki, H. Wakita, and T. Yokoyama, *J. Colloid Interface Sci.*, **2008**, *319*, 25.
63. L. R. Kump and R. H. Byrne, *Environ. Sci. Technol.*, **1989**, *23*, 663.
64. K. Tanaka, M. Tanaka, N. Watanabe, K. Tokunaga, and Y. Takahashi, *Chem. Geol.*, **2017**, *460*, 130.